Ceramics International 43 (2017) 13759–13764

Contents lists available at ScienceDirect

Ceramics International

journal homepage: www.elsevier.com/locate/ceramint

High-performance and low-voltage SnO_2-based varistors

Mateus G. Masteghin, Rafael C. Bertinotti, Marcelo O. Orlandi*

São Paulo State University (UNESP), Physical-Chemistry Department, Araraquara, SP, Brazil

ARTICLE INFO

Keywords:
B. Nanostructure
C. Electrical properties
D. SnO_2
E. Varistor

ABSTRACT

This paper presents the results of a thorough study conducted on the action mechanism of one-dimensional single-crystalline SnO_2 nanobelts in decreasing the breakdown electric field (E_b) in SnO_2-based varistors. The proposed method has general validity in that our investigation was focused on the traditional varistor composition SnO_2-CoO-Cr_2O_3-Nb_2O_5. To accomplish our study objective, two methods of decreasing E_b value were compared; one involving the increase in average grain size of the varistor through the sintering time and the other one related to the addition of nanobelts. The morphological results show that the method involving the increase in average grain size is limited by the formation of intragranular pores. Furthermore, despite contributing successfully towards decreasing the E_b value (which underwent a decline from 3990 V cm^{-1} to 1133 V cm^{-1} with an increase in sintering time from 1 h to 2 h), the reduction obtained by this method is found to be much lower compared to that obtained via the nanobelts insertion method (E_b = 270 V cm^{-1}). Impedance spectroscopy results showed that the insertion of nanobelts caused a decline in the grain boundary resistance while surface potential measurements proved that this decline in resistance is attributed to the absence of potential barriers along the belts which leads to the formation of a lower resistance percolation path in the varistor.

1. Introduction

SnO_2 is an n-type semiconductor with a Rutile-type crystalline structure. Tin dioxide has been used for several applications involving catalysts [1], photovoltaic cells [2] and gas sensor devices [3,4]. SnO_2 is a material that initially presents low density due to the evaporation/condensation processes at high temperatures. As such, for it to be employed as a varistor (which requires a high degree of densification) one needs to subject it to hot isostatic pressing sintering [5], or doping with other metal oxides with oxidation state inferior to Sn^{+4} which can promote the formation of oxygen vacancies that are responsible for controlling the mass transport during the sintering [6,7].

Cerri et al. [8] demonstrated that CoO and MnO can be employed for obtaining high-density SnO_2-based ceramics [9]. Nonetheless, high density is not the sole factor that aids in obtaining high-performance varistor ceramics. It is thus necessary to add other metal oxides, giving special preference to those with oxidation state of + 5, such as Nb_2O_5 [10,11] and Ta_2O_5 [12,13], which are known to be responsible for increasing the density of charge carriers that play a key role in the electronic transport across the grain boundaries.

Pianaro et al. [10] reported to have obtained a nonlinear coefficient (α) of 8 and a breakdown electric field (E_b) of 1870 V cm^{-1} after conducting a detailed investigation on SnO_2-CoO-Nb_2O_5 varistor system. Orlandi et al. [14] and Masteghin et al. [15] also showed that the SnO_2-MnO_2-Nb_2O_5 system can present a nonlinear coefficient (α) of 11 with a breakdown electric field (E_b) of 8786 V cm^{-1}.

Besides the aforementioned works, numerous research groups have been studying a wide range of varistor compositions based on SnO_2 [16]. Interestingly, one of the most effective results reported in the literature was also that of Pianaro et al. [10,11], which consisted of 98.90% SnO_2 – 1.00% CoO – 0.05% Cr_2O_3 – 0.05% Nb_2O_5 sintered at 1300 °C for 1 h. They reported to have obtained a nonlinear coefficient of 41 and a breakdown electric field of 3990 V cm^{-1}. The results they obtained for this composition drew wider attention for the fact that it presented a degree of effectiveness fairly capable of competing with the ZnO-based varistor containing 97.0% ZnO – 0.5% Bi_2O_3 – 0.5% CoO – 0.5% MnO – 0.5% Cr_2O_3 – 1.0% Sb_2O_3 [17].

SnO_2-based varistors present a few remarkable advantages over the ZnO-based ones. Some of these merits worth mentioning include the fact that they are single phase and inert in acidic and basic environments, making them essentially ideal for outdoor applications. The good electrical properties exhibited by ZnO-based varistors include the multiple phases found in such systems – spinel ($Zn_7Sb_2O_{12}$), pyrochlore ($Zn_2Bi_3Sb_3O_{14}$) and a polymorphic phase of bismuth oxide which contribute towards diminishing their lifetime. One drawback that was usually attributed to the SnO_2 system was the high breakdown

* Correspondence to: 55 Prof. Francisco Degni St., Araraquara 14800-060, Brazil.
E-mail address: orlandi@iq.unesp.br (M.O. Orlandi).

http://dx.doi.org/10.1016/j.ceramint.2017.07.089
Received 4 June 2017; Received in revised form 11 July 2017; Accepted 11 July 2017
Available online 12 July 2017

electric field stemming from the high number of effective potential barriers at the grain boundaries [18].

Recently, Masteghin et al. [19] presented a facile way of reducing the breakdown electric field values in SnO_2-based varistors by incorporating one-dimensional SnO_2 nanobelts in the composition, thereby rendering this new system applicable in medium and low voltage networks by virtue of the large length of the nanobelts. The results showed that this approach contributed significantly towards decreasing the breakdown electric field by up to 50%.

Thus, this work presents the effects of the insertion of SnO_2 nanobelts in the traditional system studied by Pianaro et al. [10,11]. Our study shows that in dense systems and with the optimum amount of dopants segregated at the grain boundaries, both the decrease in value of the breakdown electric field and the increase in nonlinear coefficient caused by the addition of the SnO_2 nanobelts have an exciting implication of unfolding a new era of high performance SnO_2-based varistors applicable in low voltage networks. Surface potential measurements were performed using an atomic force microscope (AFM) aiming at proving the net effect of nanobelts.

2. Experimental details

The samples used in this study were prepared by the solid-state reaction method. The powder composition was (98.90%) SnO_2 – (1.00%) CoO – (0.05%) Cr_2O_3 – (0.05%) Nb_2O_5, all obtained from Sigma-Aldrich with 99.9% purity. The mixture was homogenized in an agate mortar followed by the ball milling process (using YSZ balls) in an alcohol medium. Following homogenization, the powder was forced to pass through a 200-mesh sieve. Subsequently, half of the powder was mixed with 1 wt% of SnO_2 single-crystalline nanobelts, while the other half was used without any additional processing.

The SnO_2 nanobelts were obtained via the carbothermal reduction method using the SnO_2 powder (Sigma-Aldrich, 99.9% purity) mixed with carbon black (Union Carbide, > 99% purity). Basically, 1 g of the mixture of SnO_2:C in the molar ratio of 1.5:1 was inserted in the middle of a tube furnace where the temperature was kept at 1135 °C with a constant flux of nitrogen (150 cm^3/min^{-1}) for 75 min. Above 900 °C, an oxygen counter flow of 5 $cm^3\ min^{-1}$ was inserted and maintained until the end of the synthesis so as to obtain the desired phase [4].

The powders were compacted in cylindrical discs, with 7.0 mm of diameter and 2.0 mm of thickness, by uniaxial pressing (10 MPa), and were subsequently subjected to isostatic pressing at 150 MPa. Afterwards, the samples without belts were sintered at 1300 °C for 15, 30, 45, 60, 90 and 120 min in order to monitor the grain growth evolution using a heating and cooling rate of 10 °C min^{-1} in atmospheric air. The samples containing nanobelts were sintered for 120 min aiming at comparing their electrical properties with those of the system without belts. Samples from all systems were prepared in triplicate and polished until both sides became flat and parallel.

The structural characterization of the samples was carried out by X-ray diffraction (XRD) using Cu-Kα radiation (Shimadzu, XRD 6000). For the morphological characterizations, the samples received a final polish until obtaining a glossy surface. The grain boundaries were revealed by subjecting the samples to heat treatment at 1250 °C for 20 min. Electron microscopy analysis of all the samples was conducted on a dual beam microscope (FEI, model Helios NanoLab 600i) and the grain size analysis was made using the linear intercept method considering at least 300 grains [20]. Atomic Force Microscopy (AFM) and Kelvin Probe Force Microscopy (KPFM) measurements were carried out in a Park NX10 AFM, using a scan rate of 0.10 Hz, oscillation amplitude of 54.77 nm along with a change in the surface potential from + 5 V to − 5 V.

The electrical characterizations were carried out by direct current (*dc*) and impedance spectroscopy (*ac*) measurements. The *dc* measurements were performed using a stabilized high voltage source (Keithley, model 237), and the alternating current measurements were taken from 10 mHz to 1 MHz with a voltage amplitude of 500 mV using a frequency response analyzer (FRA32M, coupled to Autolab PGSTAT). Impedance data simulations [21,22] using an equivalent circuit were made to ascertain the grain boundary resistance of different samples.

3. Results and discussion

The structural characterization (not presented here) showed that regardless of the sintering time or the insertion of the nanobelts, the material remains single phase (at the detection limit of the equipment), presenting only the *cassiterite* phase (JCPDS #41-1445). Clearly, this result is deemed remarkable from the application point of view because having only one phase brings greater mechanical stability to the varistor and makes it easier to correlate the electrical properties with the morphological features.

One known method for reducing the breakdown electric field in varistor ceramics is by increasing the average grain size (G), which leads to a reduction in the number of potential barriers that must be overcome by the charge carriers [23]. This outcome is especially true for SnO_2-based varistors, in which the total amount of effective barriers are very high [24].

The easiest way of increasing G is by increasing the sintering time which promotes a more effective mass transport across the grain boundaries. In other words, after reaching the third stage of sintering, the grains start coarsening as a result of the difference in their interfacial energies and as part of a relaxation process [25], thus eliminating shared grain boundaries.

Fig. 1 exhibits SEM images of the samples presenting a clear increase in the average grain size (G) with the sintering time. Table 1 shows the average grain size of 2.8 μm after 15 min of sintering and 5.2 μm for 120 min of sintering, with values presenting an approximately linear increase as a function of time. This linearity is attributed to the fact that the grain size curve as a function of the sintering time is divided into linear intervals according to the fractional density of the material [25]. It is worth noting that the densities of the samples under investigation were all between 95% and 98%.

One can see from Fig. 1 that following 60 min of sintering time, a significant amount of intragranular pores appear owing to the fast mass transport through the grain boundaries, resulting in a decrease in the material density. This effect can be seen to be more evident at higher sintering times. Thus, employing greater sintering times with the aim of reducing the breakdown electric field in SnO_2-CoO-Cr_2O_3-Nb_2O_5-based varistors appears to be unfeasible once the density of the material is likely to be compromised.

In this context, the insertion of one-dimensional (1D) tin dioxide nanostructures is seen as an interesting approach for reducing the breakdown electric field. The method, which allows the use of high-performance varistors in low-voltage networks, has already proven to be reliably efficient in decreasing the number of effective barriers [19]. Fig. 2 shows SEM images of the system with inserted nanobelts prior to (Fig. 2 A) and after (Fig. 2B) sintering for 120 min.

It can be seen from Fig. 2 that the tin dioxide belts grew more than 5 times through a mechanism attributed to coalescence process, in which larger *particles* (the belts) incorporate smaller particles (the grains) when the degree of crystallographic disorientation is low (below 10 degrees), as a way of achieving equality of chemical potentials.

A further observation that deserves mentioning is that the morphology around the nanobelts remained unchanged, maintaining the average grain size of 5.2 μm following 120 min of sintering, without deleteriously altering the fractional density of the material. In fact, when the belts grow by coalescence, they eliminate grain boundaries surrounding them, enabling the migration of Co^{+2} and Cr^{+3} dopants to other boundaries, thereby allowing a better densification of the material.

Fig. 3 shows the electric field versus current density (E *vs* J) plot obtained from *dc* measurements for the samples sintered for 120 min.

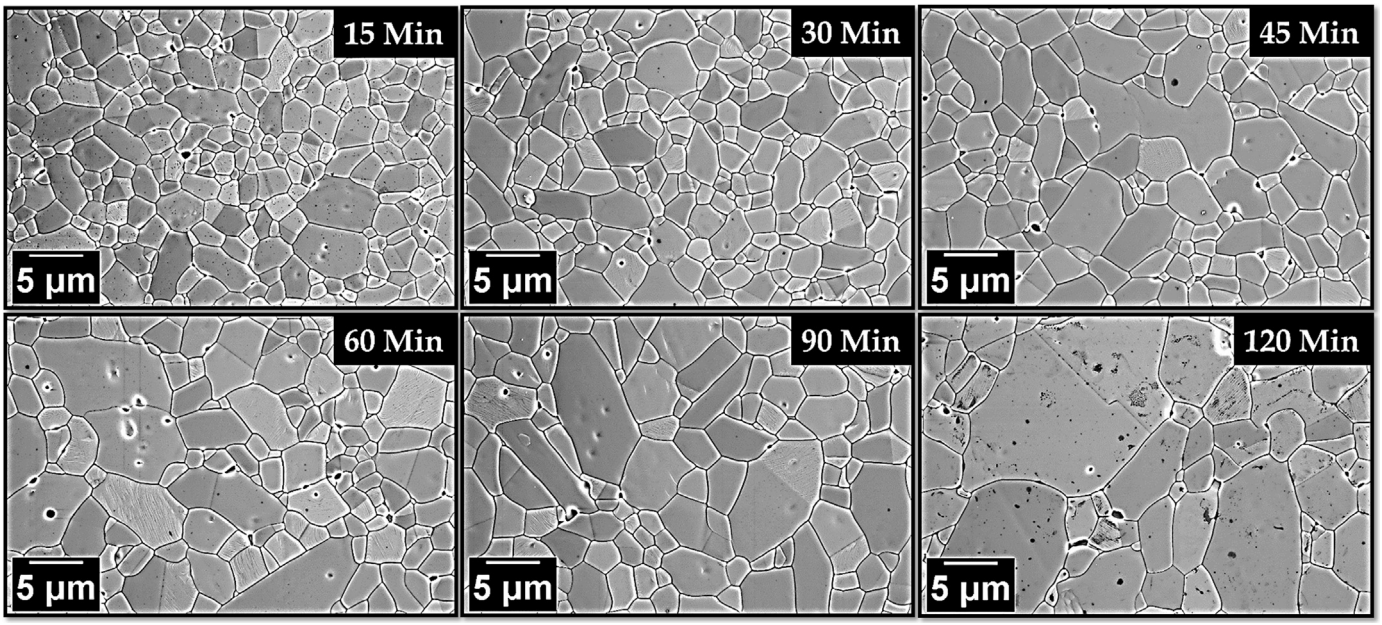

Fig. 1. SEM images of the (98.90%)SnO_2-(1.00%)CoO-(0.05%)Cr_2O_3-(0.05%)Nb_2O_5 system without nanobelts, showing the increase in the average grain size (G) as a function of the sintering time.

Table 1
Average grain size (G) as a function of sintering time for the (98.90%)SnO_2-(1.00%)CoO-(0.05%)Cr_2O_3-(0.05%)Nb_2O_5 system.

Sintering time (min)	G (μm)
15	2.8
30	3.1
45	3.4
60	3.8
90	4.5
120	5.2

The curves are found to exhibit a non-ohmic behavior for both systems while a meticulous assessment indicates a larger alpha value for samples containing nanobelts. With regard to the electric field, it is clearly noticeable that samples with belts present lower values for any current density. The nonlinear coefficient and breakdown electric field values, taken from Fig. 3, are reported in Table 2.

In this same Table 2, one can observe that increasing the sintering time without the addition of the nanobelts was sufficient to trigger an approximately 4-fold reduction in the breakdown electric field compared to the original Pianaro system [10,11] from 3990 V cm^{-1} to 1133 V cm^{-1} as a result of the increase in average grain size. On the other hand, the nonlinear coefficient was found to drop from 41 to 18

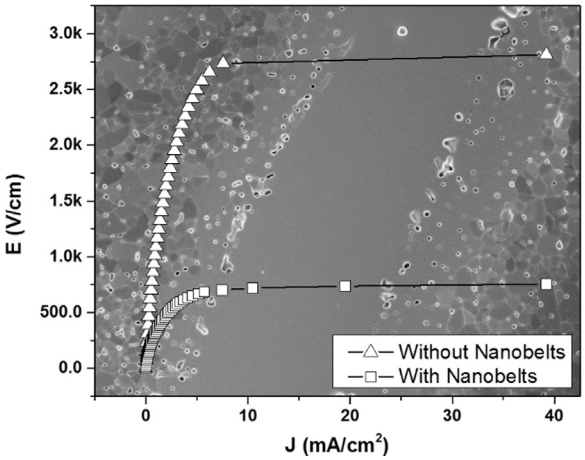

Fig. 3. Electric field (E) versus current density (J) plot of the (98.90%)SnO_2-(1.00%)CoO-(0.05%)Cr_2O_3-(0.05%)Nb_2O_5 varistor system with and without belts insertion.

[10,11], a decline of which is attributed to the reduction in the effectiveness of the potential barriers.

The addition of nanobelts triggered a drop in the breakdown electric field to 270 V cm^{-1}, which is significantly lower (75%) relative

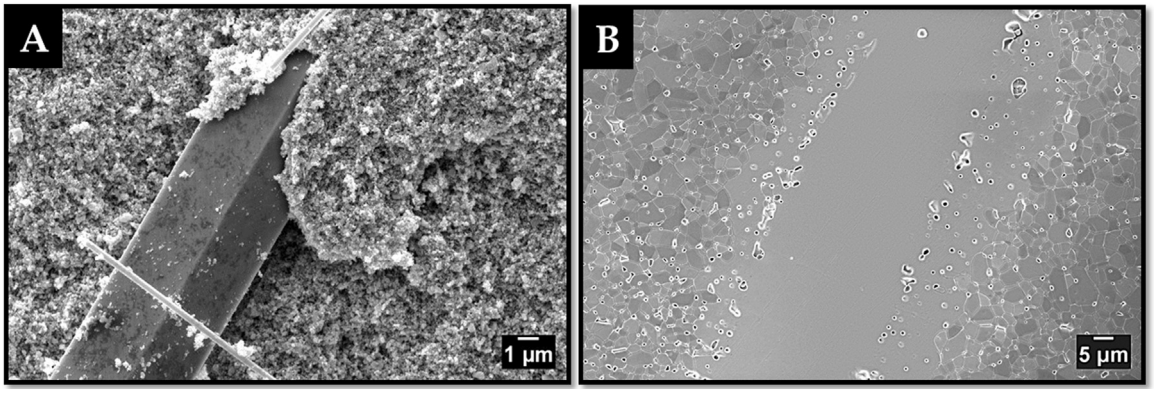

Fig. 2. (98.90%)SnO_2-(1.00%)CoO-(0.05%)Cr_2O_3-(0.05%)Nb_2O_5 system with 1% in weight of nanobelts A) Before sintering and B) After 120 min sintering.

Table 2
Nonlinear coefficient (α) and breakdown electric field (E_b) values obtained from *dc* measurements for the (98.90%)SnO_2-(1.00%)CoO-(0.05%)Cr_2O_3-(0.05%)Nb_2O_5 system, without and with 1% *wt*. of nanobelts, sintered for 2 h at 1300 °C. Values from Pianaro system [11] are included for comparison purposes.

Sample	Nonlinear coefficient (α)	E_b (V cm^{-1})
Without Nanobelts	18	1133
Pianaro et al.'s system [11]	41	3990
With Nanobelts	26	270

to the system without nanobelts. Essentially, attaining such value of E_b renders the use of this varistor system effortlessly feasible in low voltage electrical networks. This development, in effect, unfolds a new application window for high-performance SnO_2-based varistors. It is worth noting that alpha value is found to increase from 18 to 26, which is as a result of a better distribution of Co^{+2} and Cr^{+3} ions at the grain boundaries.

The decrease in E_b value is directly related to the decrease in the number of potential barriers which stems from the three-dimensional growth of nanobelts at the expense of the elimination of grain boundaries, creating numerous low electrical resistance parallel paths (*electrical shortcuts*) inside the sample.

Fundamentally, it is a well-known fact that non-ohmic properties in varistors' come from the back-to-back Schottky barrier at the grain boundaries. These barriers are formed by a depletion layer of positive charges, such as $V_O^{\cdot}$, $V_O^{\cdot\cdot}$ and $Nb_{Sn}^{\cdot}$, width ω and donor density N_d, and a negative layer composed of $O^{'}$ and $O^{''}$ species with height ϕ and surface state density (N_s), so that $N_s = 2.N_d.\omega$ [26–28]. One can infer that the nanobelts growth causes some grain boundaries to disappear while contributing towards homogenizing the segregated metals (Co^{+2} and Cr^{+3}) at other grain-grain interfaces. The adsorption of oxygen species during sintering leads to higher potential barriers (ϕ) which increase the nonlinear coefficient but without increasing the breakdown electric field due to the net effect of belts insertion.

Guided by the aim of proving the belts insertion effect, the samples were investigated using surface potential measurements with the aid of an AF microscope. Fig. 4A1 and B1 show a typical AFM topographical image of the samples without and with inserted nanobelts, respectively. The grain morphological characteristics exhibited by the materials are found to be in line with the discussion conducted on the SEM results. Fig. 4B1 shows that the belts may also present intragranular porosity due to the growth process though no potential barriers are found in them.

The capacitance gradient measurements (dC/dZ) of these samples are shown in Fig. 4A2,B2. In such measurements, the oscillation of the tip induced by the electrostatic force at the second harmonic of a non-resonant frequency is proportional to this dC/dZ gradient. This relates the measurements directly to the relative permittivity (ε_r)[29]. Hence, brighter areas represent higher dielectric constant ($k = \varepsilon_r$). This evidently demonstrates that the potential barriers are mainly composed of segregated cobalt oxide or cobalt stannate ($CoSnO_3$) responsible for the effectiveness of potential barriers since the relative permittivity of these materials is around 13 [30,31] while the dielectric constant of tin dioxide is about 9 [32].

Fig. 4A2 confirms that the SnO_2-based varistor sample presents a high number of effective barriers along the grain boundaries, which is important for obtaining high alpha values albeit undesirable when one's interest lies in obtaining low breakdown electric field. The same effect can be observed for the sample containing belts when one looks at the region devoid of belts (left side of Fig. 4B2). However, no active barriers are present within the belts (right side of Fig. 4B2), as such electrons can go through the belts with minor electrical resistance. The macroscopic effect of this greater ease at which charge carriers cross the sample is a decrease in the breakdown electric field while maintaining good nonlinear characteristics of the system.

Impedance spectroscopy measurements were performed aiming at a further investigation of the varistor samples. The Nyquist plots of the studied ceramics are presented in Fig. 5A, which also exhibits the data simulation using the equivalent circuit shown in the inset. The equivalent circuit consists of a resistor positioned in parallel to a capacitor (named R_{gb} and C_{gb}, respectively) representing the grain boundary where both of them are placed in parallel to a resistor in series with a constant phase element (CPE) representing the internal electron trap level.

Data simulation showed that the insertion of nanobelts was responsible for decreasing the grain boundary resistance in almost one order of magnitude, from 1.2×10^6 Ω to 1.9×10^5 Ω, by virtue of the percolation paths generated by the belts. Indeed, the reduction in grain boundary resistance obtained in our investigation is quite close to

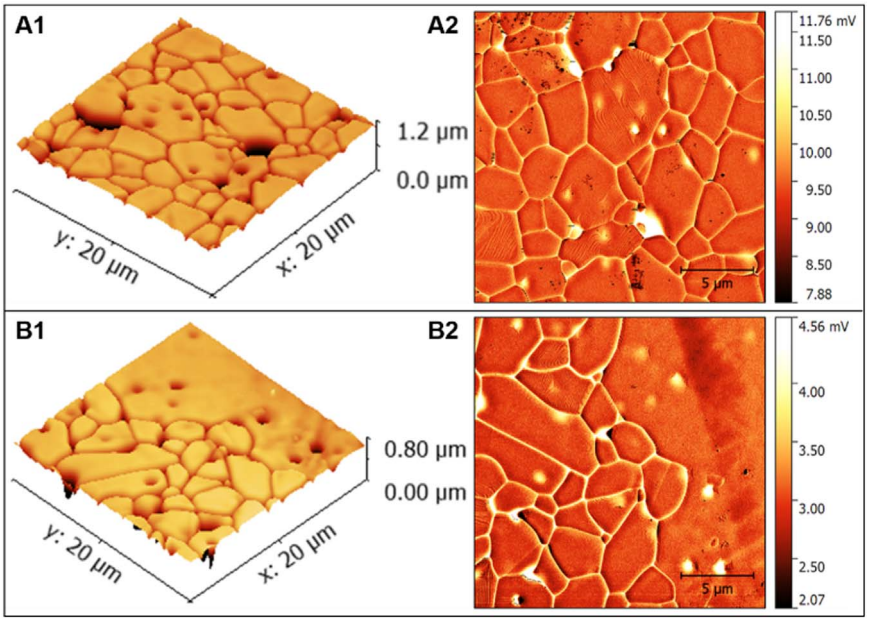

Fig. 4. A1) Topography and B1) Capacitance gradient measurement (dC/dZ) of the sample without nanobelts. A2) Topography and B2) Capacitance gradient measurement (dC/dZ) of the sample with added belts (1 wt%).

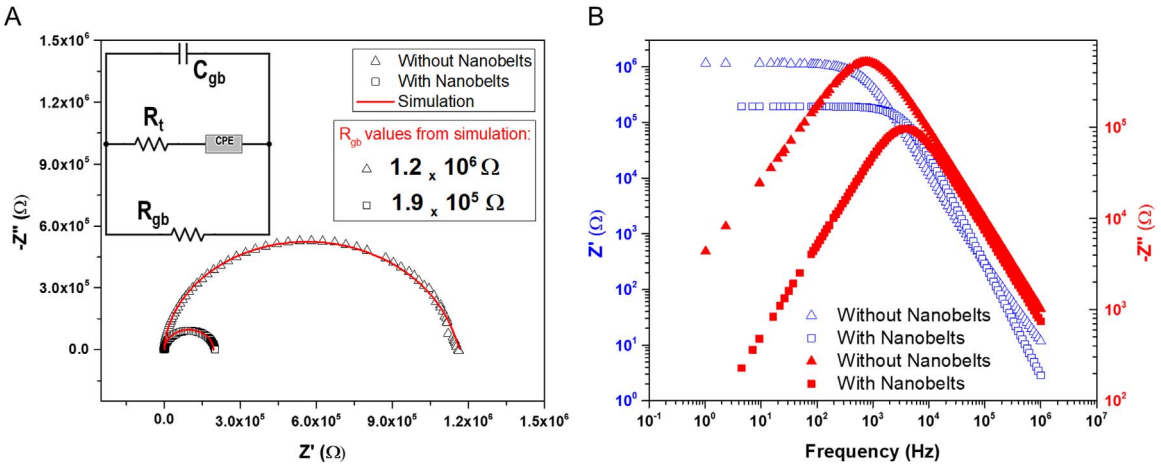

Fig. 5. A) Nyquist plots for the samples with and without inserted nanobelts. The continuous lines represent the fit made using the represented equivalent circuit. B) Real (Z′) and imaginary (Z") impedance plots as a function of frequency.

the reduction reported in previous work (in the range of 4–7 times) [19], and this reinforces the validity of the proposed model with regard to the manner in which SnO_2 nanobelts act on the electrical properties of the varistors.

The real (Z′) and imaginary (Z′′) impedance plots (Fig. 5B) allow extending the analysis based on the role played by the charge carriers. Real impedance (open symbols in Fig. 5B) results show the purely resistive behavior and a lower resistance for a system containing nanobelts. The reactance plots (solid symbols in Fig. 5B) depict all the capacitive phenomena. The results as can be observed from the plots clearly show that the system with inserted nanobelts has lower losses as a result of the decrease in the deep trap level capacitance, which is associated with higher potential barriers. Furthermore, the resonance frequency is found to be right shifted for the system with nanobelts, which implies that the electrons have greater mobility [33]. Thus, we conclude that the decrease in the number of effective barriers was essentially responsible for the higher electronic conductivity of the system with inserted nanobelts, which, in effect, reinforces the idea of larger grains.

The results presented here show that it is possible to perform defects engineering in varistor systems with excellent nonlinear properties, which, by so doing, enables their application in low-voltage networks. The breakdown electric field can be controlled by the insertion of tin dioxide nanobelts, maintaining high values of nonlinear coefficient, in other words, making the SnO_2-based varistors applicable in low-voltage networks with high performance.

4. Conclusion

The present study brought to the fore distinct ways of decreasing the breakdown electric field in a traditional SnO_2-based varistor system with a high nonlinear coefficient (α), extending its application to low-voltage electrical networks. SEM images showed that there is a limit to the increase in sintering time as a way of decreasing E_b since the varistors high density level must be preserved. The morphological study of the system with inserted monocrystalline belts exhibited a three-dimensional structural growth. The electrical measurements showed that the percolation paths generated were effective in reducing the breakdown electric field (E_b) as a result of the elimination of the potential barriers which in turn contributed towards a decline in the grain boundary resistance (R_{gb}). Surface potential measurements, which were carried out as a complementary support to the investigation, show that the region containing the belts is completely free of segregated metals.

Acknowledgments

The authors would like to thank the funding agencies FAPESP [proc. #2013/07296-2 and #2015/21033-0] and CNPq [proc #447760/2014-9, #800733/2014-2 and #303542/2015-2]. The authors would like to thank the Brazilian Nanotechnology National Laboratory (LNNano/CNPEM) for access to the AFM facilities.

References

[1] T. Tarawa, S. Kataoka, T. Hattori, Y. Murakami, Supported SnO_2 catalysts for the oxidative dehydrogenation of ethylbenzene, Appl. Catal. 4 (1982) 1–4.
[2] K.L. Chopra, S. Major, D.K. Pandya, Transparent conductors-a status review, Thin Solid Films 102 (1983) 1–46.
[3] J.G. Fagan, R.W. Amarakoon, Reliability and reproducibility of ceramic sensors. III: humidity sensors, Am. Ceram. Soc. Bull. 72 (1993) 119–130.
[4] P.H. Suman, A.A. Felix, H.L. Tuller, J.A. Varela, M.O. Orlandi, Comparative gas sensor response of SnO_2, SnO and Sn_3O_4 nanobelts to NO_2 and potential interferents, Sens. Actuators B Chem. 208 (2015) 122–127.
[5] S.J. Park, K. Hirota, H. Yamamura, Densification of nonadditive SnO_2 by hot isostatic pressing, Ceram. Int. 11 (1985) 158.
[6] J.A. Aguilar-Martínez, P. Zambrano-Robledo, S. García-Villarreal, M.B. Hernández, E. Rodríguez, L. Falcon-Franco, Effect of high content of Co_3O_4 on the structure, morphology, and electrical properties of (Cr, Sb)-doped SnO_2 varistors, Ceram. Int. 42 (2016) 7576–7582.
[7] O.A. Desouky, K.E. Rady, Synthesis, structure and dielectric properties of nano-crystalline SnO_2–CoO–Nb_2O_5 varistor doped with Cr_2O_3, J. Mater. Sci. Mater. Electron. 28 (2017) 1–7.
[8] J.A. Cerri, E.R. Leite, D. Gouvêa, E. Longo, J.A. Varela, J.A. Eff1. Cerri, E.R. Leite, D. Gouvêa, E. Longo, J.A. Varela, Effect of Cobalt(II) Oxide and Manganese(IV) Oxide on sintering of Tin(IV) Oxide, J. Am. Ceram. Soc. 79 (1996) 799–804.
[9] J.A. Varela, J.A. Cerri, E.R. Leite, E. Longo, M. Shamsuzzoha, R.C. Bradt, Microstructural evolution during sintering of CoO doped SnO_2 ceramics, Ceram. Int. 25 (1999) 253–256.
[10] S.A. Pianaro, P.R. Bueno, E. Longo, J.A. Varela, A new SnO_2-based varistor system, J. Mater. Sci. Lett. 14 (1995) 692–694.
[11] S.A. Pianaro, P.R. Bueno, E. Longo, J.A. Varela, Microstructure and electric properties of a SnO_2 based varistor, Ceram. Int. 25 (1999) 1–6.
[12] A.C. Antunes, S.R.M. Antunes, S.A. Pianaro, M.R. Rocha, E. Longo, J.A. Varela, Nonlinear electrical behaviour of the SnO_2·CoO·Ta_2O_5 system, J. Mater. Sci. Lett. 17 (1998) 577–579.
[13] A.Z. Simões, A. Ries, L. Perazolli, E. Longo, J.A. Varela, Nonlinear electrical behaviour of the Cr_2O_3, ZnO, CoO and Ta_2O_5-doped SnO_2 varistors, Ceram. Int. 32 (2006) 283–289.
[14] M.O. Orlandi, M.R.D. Bomio, E. Longo, P.R. Bueno, Nonohmic behavior of SnO_2-MnO polycrystalline ceramics. II. Analysis of admittance and dielectric spectroscopy, J. Appl. Phys. 96 (2004) 3811–3817.
[15] M.G. Masteghin, M.O. Orlandi, Grain-boundary resistance and nonlinear coefficient correlation for SnO_2-based varistors, Mater. Res. 19 (2016) 1286–1291.
[16] G.Z. Zang, X.F. Wang, L.B. Li, D.D. Wang, The effect of Sm_2O_3 on the microstructure and electrical properties of SiO_2-doped SnO_2-Zn_2SnO_4 ceramic varistors, Ceram. Int. (2017).
[17] M. Matsuoka, Nonohmic properties of zinc oxide ceramics nonohmic properties of zinc oxide ceramics, Jpn. J. Appl. Phys. 10 (1971) 736–746.
[18] P.R. Bueno, E.R. Leite, M.M. Oliveira, M.O. Orlandi, E. Longo, Role of oxygen at the grain boundary of metal oxide varistors: a potential barrier formation mechanism, Appl. Phys. Lett. 79 (2001) 48–50.

[19] M.G. Masteghin, J.A. Varela, M.O. Orlandi, Controlling the breakdown electric field in SnO_2 based varistors by the insertion of SnO_2 nanobelts, J. Eur. Ceram. Soc. 37 (2017) 1535–1540.
[20] M.I. Mendelson, Average grain size in polycrystalline ceramics, J. Am. Ceram. Soc. 52 (1969) 443–446.
[21] B.A. Boukamp, A nonlinear least squares fit procedure for analysis of immittance data of electrochemical systems, Solid State Ion. 20 (1986) 31–44.
[22] B.A. Boukamp, A package for impedance/admittance data analysis, Solid State Ion. 18 (1986) 136–140.
[23] E.R. Leite, A.M. Nascimento, P.R. Bueno, E. Longo, J.A. Varela, Influence of sintering process and atmosphere on the non-ohmic properties of SnO_2 based varistor, J. Mater. Sci. Mater. Electron. 10 (1999) 321–327.
[24] J.S. Vasconcelos, N.S.L.S. Vasconcelos, M.O. Orlandi, P.R. Bueno, J.A. Varela, E. Longo, C.M. Barrado, E.R. Leite, Electrostatic force microscopy as a tool to estimate the number of active potential barriers in dense non-Ohmic polycrystalline SnO_2 devices, Appl. Phys. Lett. 89 (2006).
[25] R.M. German, Coarsening in sintering: grain shape distribution, grain size distribution, and grain growth kinetics in solid-pore systems, Crit. Rev. Solid State Mater. Sci. 35 (2010) 263–305.
[26] D.R. Clarke, Varistor ceramics, J. Am. Ceram. Soc. 82 (1999) 485–502.
[27] T.K. Gupta, Application of zinc oxide varistors, J. Am. Ceram. Soc. 73 (1990) 1817–1840.
[28] E.R. Leite, J.A. Varela, E. Longo, A new interpretation for the degradation phenomenon of ZnO varistors, J. Mater. Sci. 27 (1992) 5325–5329.
[29] W. Melitz, J. Shen, A.C. Kummel, S. Lee, Kelvin probe force microscopy and its application, Surf. Sci. Rep. 66 (2011) 1–27.
[30] K.V. Rao, A. Smakula, Dielectric properties of cobalt oxide, nickel oxide, and their mixed crystals, J. Appl. Phys. 36 (1965) 2031–2038.
[31] W.W. Coffeen, Ceramic and dielectric properties of the stannates, J. Am. Ceram. Soc. 36 (1953) 207–214.
[32] H.J. Van Daal, The static dielectric constant of SnO_2, J. Appl. Phys. 39 (1968) 4467–4469.
[33] V.P.B. Marques, M. Cilense, P.R. Bueno, M.O. Orlandi, J.A. Varela, E. Longo, Qualitative evaluation of active potential barriers in SnO_2-based polycrystalline devices by electrostatic force microscopy, Appl. Phys. A 87 (2007) 793–796.